Modeling high current events for solar inverters with subhourly data

Mónica Zamora Zapata,[1] Kari Lappalainen,[2] Adam Kankiewicz,[3] and Jan Kleissl[4]

[1)]*Departamento de Ingeniería Mecánica, Universidad de Chile, Chile*

[2)]*Unit of Electrical Engineering, Tampere University, Finland*

[3)]*Black & Veatch, USA*

[4)]*Department of Mechanical and Aerospace Engineering, University of California San Diego, USA*

(*mzamora@uchile.cl.)

(Dated: 16 March 2023)

Inverter string design and selection are crucial steps in solar photovoltaic design. The input of an inverter varies with the solar resource and weather conditions; therefore, a good design must ensure that the input current is within the rated values. Traditional design calculations estimate the maximum current either as 125% of the rated module current or as the maximum 3 hour average current from hourly simulations over a typical year. Hourly simulations neglect the most extreme irradiance conditions, which are cloud enhancement events that usually last minutes. In this study, we use 10 years of 1 minute data from 7 stations across the United States to model inverter input (short-circuit current and maximum-power point current), observing the effect of temporal resolution and averaging. We consider different configurations: minutely to hourly resolution; 5 min to 3 h averaging time intervals; monofacial and bifacial modules (with a case of enhanced albedo); and 3 fixed-tilt angles and horizontal single-axis tracking. The bifacial modules with enhanced albedo lead to the highest currents for 1 min data, corresponding to 53% or 38% higher than 3 hour averages, respectively. The 3 hour average maxima surpass the conservative 125% design rule for bifacial modules. While 1 min maxima occurred at Sioux Falls, extreme events were more frequent and lasting longer at Boulder and Desert Rock. If 1 min events that exceed the inverter rating are undesired, either a 200% rule or 1.55 times the 3 hour maximum average, as derived from hourly data, are recommended.

I. INTRODUCTION

Solar photovoltaic (PV) plants have grown strongly in the past decade, reaching 738 GW of installed capacity worldwide in 2021, and capacity is expected to double in the next 5 years[1]. As solar penetration continues to grow, one of the main challenges for grid integration is the variability of the solar resource, where not only diurnal cycles matter but also the quick changes that can occur due to passing clouds. Clouds usually diminish the solar irradiance reaching the surface but clouds can also augment it, in a process known as cloud or irradiance enhancement.

Irradiance enhancement typically occurs during broken cloud sky conditions[2], and is caused by forward scattering on thin clouds and reflection on the sides of thick clouds[3,4]. While locations with high elevation near the Equator are expected to yield stronger values, measurements of overirradiance events have been reported all over the world. The peak measurements include 1891 W/m^2 in Colorado, USA[5] and 1845 W/m^2 in Brazil[2]; higher latitudes are not free of these events: 1528 W/m^2 were measured in Norway[6]. All these strong values highly surpass the standard testing conditions of 1000 W/m^2 for PV modules, and can result in high output currents as well as power, both of which also depend on the operating module temperature[7,8]. The duration of the irradiance enhancement events can last from seconds to minutes[2,6,7], while their spatial coverage can span multiple kilometers[9], which poses a problem for utility scale PV plants.

Inverters and the inverter string design (i.e., how many solar modules to connect in parallel) must be selected such that the weather conditions at the site of interest will not impact its fault-free operation. In particular, we focus on blown fuses, which occurs when the current exceeds the fuse rating. Fuses exist in combiner boxes after the PV modules as well as on inverter DC inputs, and they must sustain temperatures of up to 80ºC that develop inside IP rated enclosures, which can diminish the inverter lifetime[10], and reduce the admissible current of fuses by factors of around 0.8[2]. Some inverters also have software limitations which limit DC feeder current limits in addition to mechanical fuse protection, and in case of an overcurrent, a major inverter fault occurs. Blown fuses and inverter faults have been observed in several operational PV plants recently[2], and are a major maintenance issue as both require manual intervention; the fuses have to be replaced, and inverters need to be reset, and there is typically no on-site staff.

There are two main reasons why the verification of weather conditions not impacting the operation could be fallible. The first is the temporal resolution of the weather data. Irradiance enhancement events tend to last seconds or minutes[2,11,12], while solar PV design usually considers

hourly data, completely missing the quick changes that can lead to blown fuses. A second reason that contributes to a higher risk of damage is the recent trend of increasing inverter loading ratios (ILR or DC/AC ratio) due to the declining costs of PV modules. Increasing ILR means connecting more PV modules to an inverter, which results in "clipping" or losing some power when the output of the PV modules surpasses the inverter power capacity on bright days. These losses are thought to be compensated by a higher production during winter months and in cloudy conditions. Recent measurements in Brazil suggest the opposite: undersized inverters can result in a lower annual energy generation due to overheating[10].

The effect of time resolution has gained attention in the context of energy clipping. Kharait et al.[13] used 1 month of 1 minute measurements at the NIST testing site in Gaithersburg, MD, to predict energy yield and clipping losses for ILRs of 1.1, 1.3, and 1.5. Simulations in SolarFarmer showed that energy yield grows while clipping losses diminish with coarser time resolution and lower ILR, and that sensitivities are larger with higher ILR. Parikh et al.[14] expanded this study at the same site, for PV systems with tracking and ILR of 1.43. They used machine learning models to apply clipping loss correction factors on hourly data, reducing the PV generation bias error. Similarly, Anderson and Perry[15] used 29 ground stations in the US with 1 min solar data, and calculated correction factors for the clipping error of 30 min satellite data. This dataset was then used to train machine learning predictions in order to create a correction factor map for the whole continental US. This study considered a PV system with a fixed tilt of 20º and ILR of 1.4. Other than clipping, Luoma et al.[11] used 1 second resolution data in San Diego, CA, to predict energy losses due to the effect of time resolution on the effective inverter efficiency, showing that 10 second resolution is needed to capture the losses related to cloud enhancement events.

So far, these studies have not covered over-current issues. The industry standard for verifying inverter input conditions is described by Ladd[16] in a SolarPro article. While the NEC 1999 rule introduced a 125% multiplier, meaning that the minimum short-circuit current for selecting an inverter would be 1.25 times the short-circuit current of the PV module, the NEC 2017 rule allows simulating the local conditions on the PV modules and then using the highest 3 hour average of the modeled short-circuit current as the maximum operating condition (as long as it is higher than 70% of the value obtained with the 125% multiplier). But a 3 hour average will neglect cloud enhancement events. To examine whether existing design rules are appropriate, there is a need to use high resolution data and report the strength and frequency of these high current events. The issue of high currents is expected to be of greater importance for bifacial modules. There is a

brief mention of over-currents for bifacial modules in the IEA Task 13 report[17], where estimates of maximum PV module current at 1 min resolution were reported to be 42% higher than the maximum 3 hour average, considering fixed tilt conditions at 3 sites in the US.

In this work, we study the effect of time resolution on simulated inverter input current, and compare it to the industry standard calculations. We compare results for 10 years of data with 1 minute resolution to results from downsampled time series for longer time intervals at 7 SURFRAD sites in the continental US. Simulations are run in pvlib for two PV system configurations with standard and bifacial modules, considering three tilt angles as well as horizontal single axis tracking for a total of 12 scenarios. The paper is structured as follows: Section II describes the data, PV systems, and the methods. Section III shows the simulated results and their comparison to current industry standards, reporting the frequency and duration of extreme events. Section IV contains the conclusions.

II. DATA AND METHODS

A. Solar and weather data

We use solar and meteorological data from 7 SURFRAD stations: Bondville, IL, Boulder, CO, Desert Rock, NV, Fort Peck, MT, Goodwin Creek, MS, Penn State, PA, and Sioux Falls, SD; corresponding to different climate conditions in the continental US. The data has 1 minute resolution, and we use historical records spanning 10 years from 2011 to 2020. The data is downsampled to coarser time resolutions of 5, 15, 30, and 60 minutes.

B. PV systems

We use two reference PV systems for our simulations including monofacial and bifacial modules. Since our focus is on inverter input conditions, our results will consider the output of a single PV string. Typically, inverters are connected to several strings with similar setup of PV modules that are wired in parallel or in series. Traditionally, strings had been identical for ease of design and construction, but strings are becoming more heterogeneous as more projects are developed in complicated terrains. Each string is protected by a separate fuse. Therefore a string is the relevant unit for examining over-currents.

The first PV system, representing the monofacial case, is taken from Ladd[16], with a total capacity of 120 kW consisting of 4 inverters of 30 kW. Each inverter is fed by 5 strings of 19 Yingli YL330P-35b modules connected in series. The ILR for this system is 1.05, and the inverter has a maximum input voltage of 1,000 V and a maximum operation current of 66 A (13.2 A per string in our case). The Yingli PV module has a 15 A fuse.

The second PV system, representing the bifacial cases, is taken from Ayala Pelaez et al.[18]; it is a 200 kW DC system with 6 Chint 36 kW inverters. The bifacial modules are Silfab 285 W, and no details were reported regarding the number of modules per string nor the number of strings connected to the inverter, so we assume that each inverter is fed by 5 strings of 19 Silfab modules in series leading to 570 modules in total. Assuming a high bifacial gain (BG) of 15%, attainable in a single-axis tracking configuration for an albedo of 0.4[19], the module power gives an estimated ILR of 0.84 which is low. The inverter has a maximum input voltage of 1,000 V and for 5 strings it allows a maximum input current of 14 A per string. This inverter has a 15 A fuse.

Each PV system is simulated for the following configurations. We consider 3 fixed-tilt angles and a case with horizontal single axis tracking (HSAT). The fixed-tilt angles are 10º, 25º, and an optimal tilt for each site. The optimal tilt corresponds to the angle that maximizes the energy yield for the monofacial module in the year 2020. The values obtained for each site are: Bondville, IL: 33º, Boulder, CO: 37º, Desert Rock, NV: 35º, Fort Peck, MT: 40º, Goodwin Creek, MS: 30º, Penn State, PA: 32º, and Sioux Falls, SD: 38º. For the bifacial modules, two albedo scenarios are considered: the annual mean of each site[20], and an improved white painted concrete of 60%[21], as done in the IEA Task 13 report[17]. This enhanced albedo may not be realistic for traditional PV design, but we have included it to represent an extreme condition.

C. Simulation and current variables

We model the output from the PV modules using pvlib[22]. Measured direct and diffuse solar irradiance is transformed to the plane of array using the Perez transposition model, and, depending on the case, either annual mean values of albedo or an enhanced albedo of 0.6 are given for the ground diffuse component[20]. Since both modules are in the CEC database, module output is obtained with the single diode CEC model, which calculates the cell temperature using the NOCT (Nominal Operating Cell Temperature). Following Ladd[16], all possible losses are set to zero (electrical, soiling, shading, and snow), representing the worst case scenario for current out-

put. For the bifacial system, the rear side irradiance is obtained with pvfactors, a 2D method for calculating the view factors for the back side irradiance[23]. For bifacial irradiance, only data for elevation angles greater than 10º was considered for the search of maximum current, since some early times resulted in unrealistic high values. Eliminating these values is not expected to exclude real maximum currents since the highest overirradiance events occur near noon[24].

To compare our results with industry standards, we define the following output variables. The 125% multiplier from the NEC 2009 rule is applied to the module short-circuit current, $I_{sc,mod}$, which in these cases are 9.29 A for the Yingli and 9.49 A for the Silfab module: $I_{125\%} = 1.25 \cdot I_{sc,mod}$, corresponding to 11.61 A and 11.86 A, respectively.

In practice, we would use $I_{125\%}$ as the maximum operating condition per string to select an inverter. To reduce inverter cost, the NEC 2017 code allows reducing the conservative 125% value using a 3 hour average of simulated performance. We obtain the modeled (actual) short-circuit current with the single diode CEC model from pvlib: I_{sc}. In Ladd[16], the short-circuit current was corrected using the cell temperature. Both methods yield similar results but their values are sensitive to the module temperature coefficients α_{sc} and β_{oc} (not shown), which can slightly differ between the datasheet (used by Ladd) and the CEC database (used in pvlib). For consistency and reproducibility we use the CEC database and pvlib built-in methods. We also report values of the current at the maximum-power point, I_{mp}, which represents typical operational conditions.

The NEC 2017 rule suggests using the maximum 3 hour average of the modeled short-circuit current, $I_{sc,3h}$. We will compare the average modeled short-circuit current and maximum-power current for different input data time resolutions as well as different averaging time windows: 5 min, 15 min, 30 min, 1 h and 3 h, for each of the sites, tilts, and module configurations.

III. RESULTS

A. Sample results

Fig. 1 shows the solar resource and the modeled short-circuit current (I_{sc}) as well as the maximum-power point current (I_{mp}) for May 12, 2020, at Sioux Falls, SD. This day has strong variability, and irradiance enhancement events between 15:00-22:00 UTC.

The modeled I_{sc} and I_{mp} currents are shown for the 25º tilt configuration (Fig. 1b-d), which closely follows the global horizontal irradiance (GHI, Fig. 1a), while the HSAT results (Fig. 1f-h)

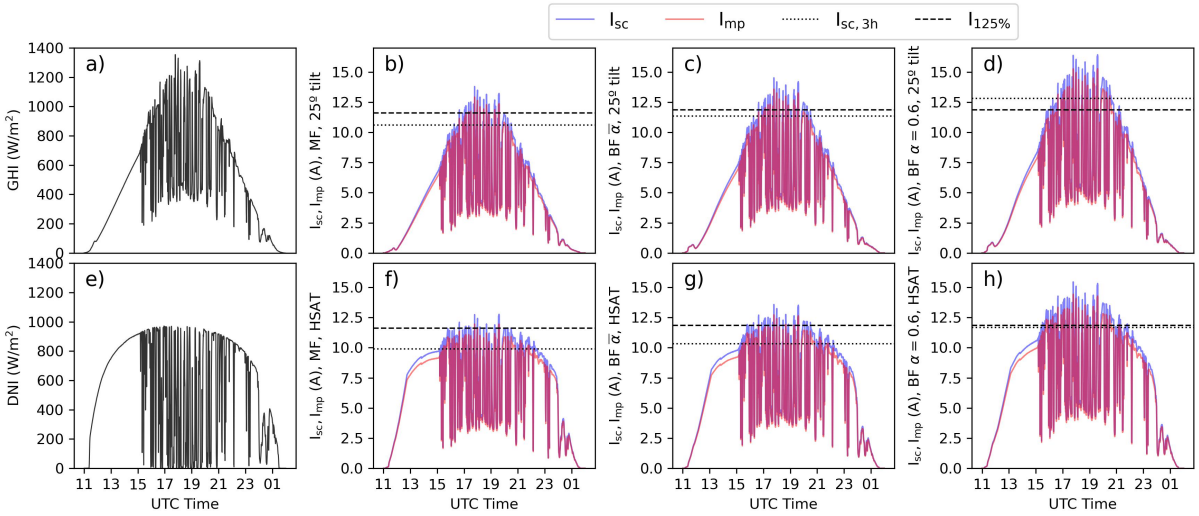

FIG. 1. Solar irradiance and modeled output currents for May 12, 2020 at Sioux Falls, showing strong variability for a large portion of the day. The first column shows the solar irradiance components: a) GHI (global horizontal irradiance) and e) DNI (direct normal irradiance). The modeled maximum-power point (red) and short-circuit (blue) currents are shown in the rest of the panels. The first row b-d) shows the values for the 25º tilt configuration and the second row f-h) for the HSAT configuration. The panels in the last three columns correspond to different module setups: b,f) show monofacial, c,g) bifacial with mean albedo, and d,h) bifacial with $\alpha = 0.6$. Horizontal lines correspond to the maximum current selected according to the 125% rule (dashed) and the maximum 3 hour average short-circuit current for the site (dotted).

resemble more the direct normal irradiance (DNI, Fig. 1e). The short-circuit current, I_{sc}, is by definition always greater than the maximum-power point current, I_{mp}. The modeled currents are amplified with bifacial modules, even more so when the albedo is enhanced, since the effective irradiance reaching the modules increases. With tracking, the current peaks are lower than those of the 25º fixed-tilt system throughout the day because horizontal tracking occurs at a suboptimal tilt angle. If we had considered tilted tracking, it would have resulted in more extreme values but two-dimensional tracking is uncommon for utility-scale plants. Lastly, the dashed and dotted lines show the selected maximum current by using the 125% rule and the 3 hour average, respectively. The current peaks do surpass the industry standards at times, and can even be greater than 15 A, the fuse rating, for some configurations. Lastly, we note that the maximum 3 hour average can be greater than the 125% rule for the bifacial modules with enhanced albedo.

B. Maximum expected current and time resolution

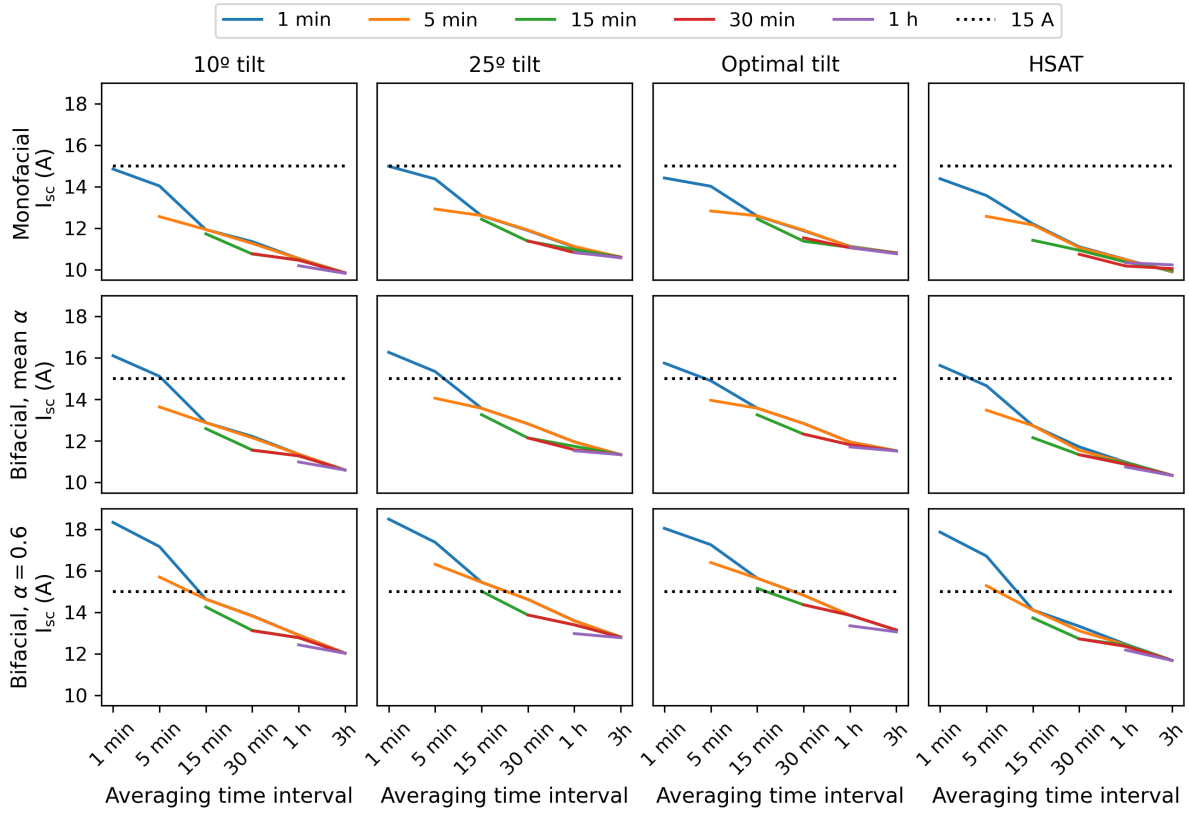

FIG. 2. Maximum short-circuit current I_{sc} for Sioux Falls, obtained from the different downsampled timeseries (1 min to 1 h), are shown as a function of the averaging time interval (1 min to 3 h).

The effect of time resolution and the averaging time interval on the maximum I_{sc} is shown in Fig. 2 for Sioux Falls. All sites show a similar behavior: the maximum currents decrease when increasing the averaging time interval, as expected. Meanwhile, for the same averaging time interval, the maximum currents found for coarser time resolution are lower or equal than the maximum found for the 1 minute averaged at that time interval. This is also expected since the downsampled timeseries may lose some extreme information while the 1 minute averaged timeseries will always contain the highest peaks, leading to the highest possible maximum.

In other words, coarser time resolution can underestimate the maximum values, and averaging with longer time windows certainly underestimates them. However, the difference of time resolution is minor when looking at 3 hour statistics, meaning that the maximum value of the 3 hour average, used for the NEC 2017 rule, is virtually identical if the original data has 1 minute or

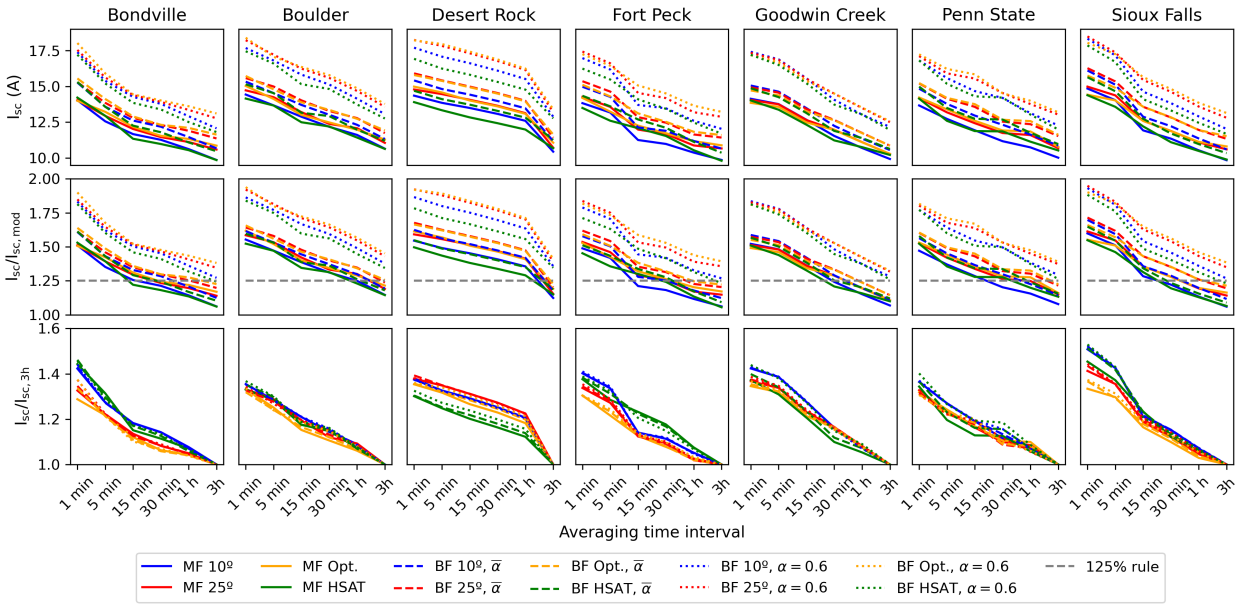

FIG. 3. Maximum short-circuit current I_{sc} as a function of the averaging time interval by site, using the 1 minute resolution data. The top row shows the absolute values, the middle row shows the values normalized by the module short-circuit current $I_{sc,mod}$ with the 125% NEC in dashed gray. The bottom row shows the values normalized by the 3 h average maximum.

1 hour resolution. The behavior of I_{sc} and I_{mp} is similar, with the latter being always lower by around 1.5 A (see Appendix A for complementary figures).

Bifacial modules reach a higher current than monofacial ones, and the enhanced albedo creates the strongest maxima for the 25º tilt. The way in which maximum currents decrease with coarser averaging time intervals is unique for each site. Some sites show a more linear behavior while others suddenly decrease at a specific averaging time interval. In the case of Sioux Falls (and also Fort Peck in Fig. 3), the sudden decrease occurs between the 5 and 15 minute intervals. This difference suggests that there is a characteristic timescale related to the duration of the strong current events for each site, which is likely to be related to the features of the clouds that lead to the strongest irradiance enhancement events at each location. Fig. 3 shows that the longest timescale is seen for Desert Rock, where the change of slope occurs at the averaging time interval of 1 h.

Fig. 3 presents the results of the 1 minute timeseries of maximum modeled short-circuit current as a function of averaging time interval for all sites. In other words, the 12 tilt/tracking and bi/monofacial cases considered in Fig. 2 are put together in a single plot for each site. The top row in Fig. 3 shows that the maximum 1 minute short-circuit current for many configurations surpasses

the inverter nameplate limits (13.2 A for the monofacial, 14 A for the bifacial, and also the 15 A fuses for the monofacial module and the Chint inverter).

The normalized current values (second and third rows in Fig. 3) show the ratio with respect to the module's reference short-circuit current, $I_{sc,mod}$, and the ratio with respect to the 3 hour average maximum, $I_{sc,3h}$ to comparing to the NEC 2009 and NEC 2017 calculations. The same plot is included for I_{mp} in Appendix A (Fig. 7).

The ratio $I_{sc}/I_{sc,mod}$ (Fig. 3 second row) shows that for all the bifacial modules with enhanced albedo, even the maximum 3 h average is greater than $I_{125\%}$, meaning that the 125% rule is not conservative enough for those conditions. Furthermore, the 125% rule is not much greater than the 3 hour averages for Boulder and Desert Rock in the case of monofacial modules. Second, the maximum for the 1 minute data almost double $I_{sc,mod}$ for Sioux Falls (195%), Boulder (194%), Desert Rock (192%) and Bondville (190%) in the bifacial cases with enhanced albedo, while for the other cases the 1 minute maximum is at least 145% of $I_{sc,mod}$. For $I_{mp}/I_{sc,mod}$ (Fig. 7 second row), the values are less extreme but still surpass 125%: while for monofacial modules $I_{mp}/I_{sc,mod}$ ranges from 138% at Penn State to 151% at Boulder, the maximum values for bifacial modules reach 179% at Bondville and 178% at both Boulder and Desert Rock.

The bottom row in Fig. 3 shows the ratio between the maximum averaged values and the maximum 3 hour average value. Here, we see that with normalization, the curves become similar and dependent only of tilt or tracking configuration, which is expected since they determine the effective irradiance reaching the modules. The $I_{sc}/I_{sc,3h}$ ratio is greatest for the Sioux Falls site, where the 1 minute maximum is 53% greater than the maximum 3 h average, followed by Bondville (46%) and Goodwin Creek (44%), all of these values occuring for bifacial modules with enhanced albedo and a HSAT configuration. Meanwhile, the minimum occurs for monofacial modules at Bondville (29%). These values are in line with the simulated conditions and sites included in the IEA Task 13 report[17], where the same ratio reached 42% for fixed tilt conditions at 3 sites in the US. In the case of $I_{mp}/I_{sc,3h}$ (Fig. 7 bottom row), the maximum ratios reach 38% for Sioux Falls while the minimum is 20% for Penn State.

C. Frequency and duration of high current events

The fact that the 125% rule is exceeded dramatically seems concerning. However, the strength of the most extreme event in 10 years is not the only factor that affects the operation of the PV

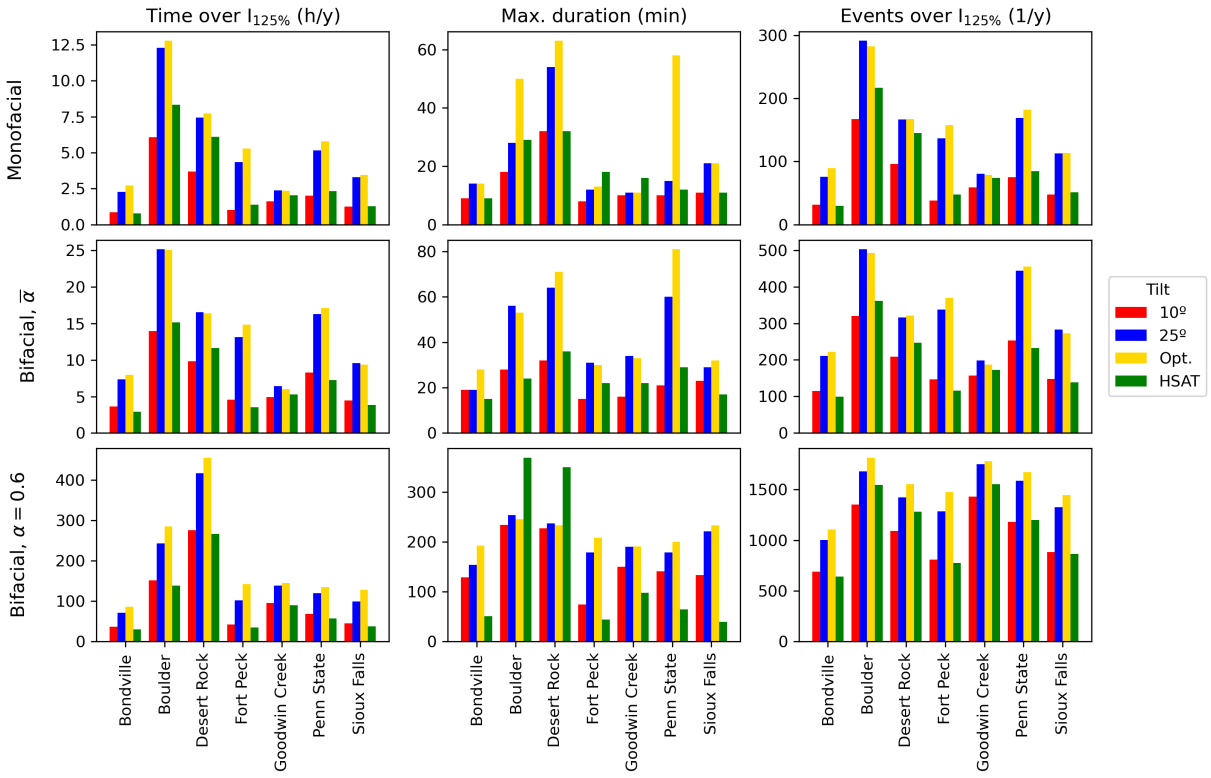

FIG. 4. Statistics of events whose short-circuit current is over the 125% rule per site and module configuration. The first column shows the time of these events per year, the second the maximum duration of the events, and the third the number of events per year. The first row corresponds to monofacial modules, the second to bifacial, and the bottom row to bifacial with enhanced albedo. The colors show the tilt or tracking configuration, with Opt. meaning optimal tilt angle.

system. Other relevant metrics are how frequent the events over the 125% rule are for each site, and how long they usually last. Figs. 4 and 5 show different statistics for the events that surpass $I_{125\%}$ based on I_{sc} and I_{mp}, with the latter being more representative of operational conditions. The statistics in each plot include: the total time above $I_{125\%}$ in hours per year (first column), the maximum duration of these events in minutes (mid column), and the number of events per year (third column).

As expected, the events occur more frequently for higher tilt angles (blue and yellow bars), and for the locations with a more abundant solar resource: Boulder and Desert Rock. While I_{sc} in a PV plant with monofacial modules at Goodwin Creek might surpass the 125% rule for around 2 hours per year, another at Boulder could reach 12 hours per year. As we change to bifacial modules with enhanced albedo, the frequency increases, reaching up to 456 hours per year at Desert Rock

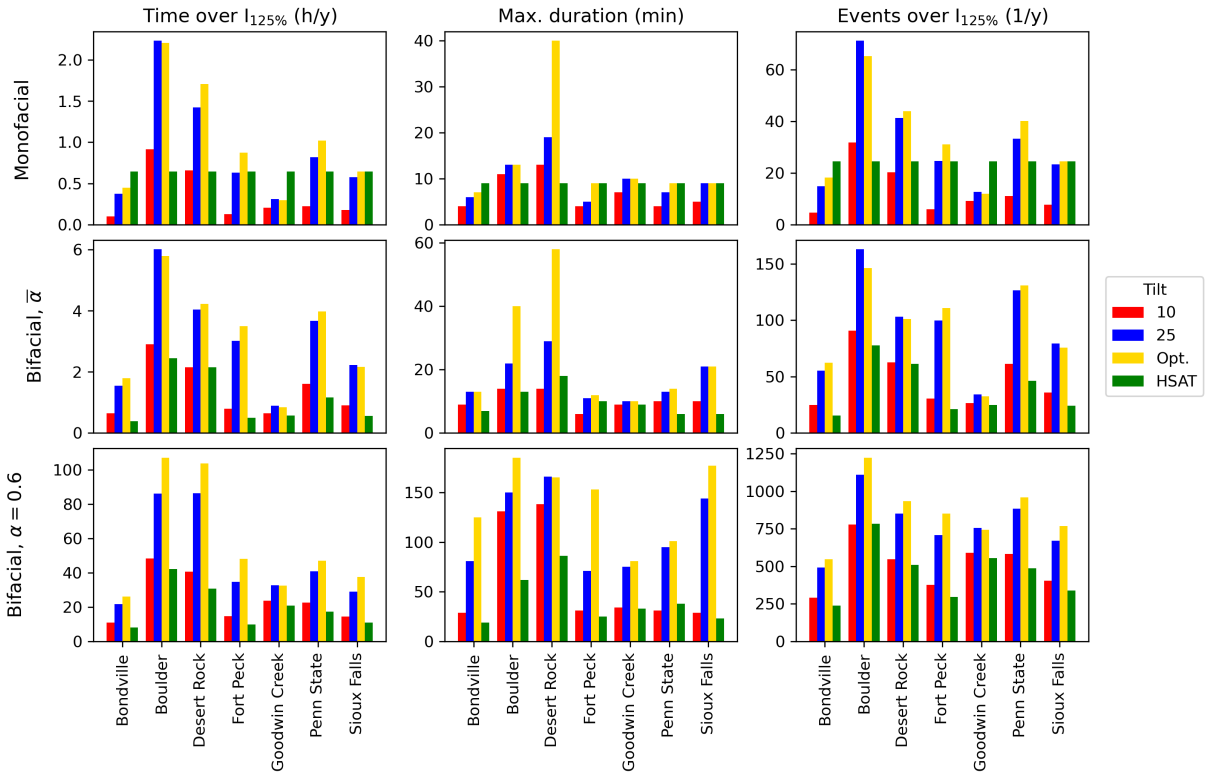

FIG. 5. Statistics of events whose maximum-power point current is over the 125% rule per site and module configuration. The first column shows the total time of these events per year, the second the maximum duration of single events, and the third the number of events per year. The first row corresponds to monofacial modules, the second to bifacial, and the bottom row to bifacial with enhanced albedo. The colors show the tilt or tracking configuration, with Opt. meaning optimal tilt angle.

(equivalent to full 38 solar days). I_{mp} in Fig. 5 gives an idea of actual operational failures. The numbers are about a third of the statistics based on I_{sc}. The worst case in monofacial modules is Boulder with only 2.2 hours per year and bifacial with enhanced albedo at 134 hours (equivalent to 5.6 days), .

In terms of duration, the longest events where $I_{sc} > I_{125\%}$ for the monofacial cases last between 8 and 63 minutes at Fort Peck and Desert Rock, respectively. For the bifacial modules with average site albedos, the range is between 15 minutes at both Bondville and Fort Peck, and 81 minutes at Penn State. Lastly, the bifacial modules with enhanced albedo result in the longest events between 39 minutes for Sioux Falls and 369 (over 6 h) at Boulder, which are probably not related to irradiance enhancement but extended favorable conditions. In fact, note that the longest events for enhanced albedo occur at Boulder and Desert Rock for the HSAT configurations, meaning

that tracking is playing an important role in augmenting the incident irradiance over the modules throughout the day, not just for irradiance enhancement events but mean irradiance as well. The extreme events based on $I_{mp} > I_{125\%}$ show a similar behavior, but note that in these cases the longest events are not for the HSAT configuration. Here, the longest events last 40 min for the monofacial modules at Desert Rock, 58 min for the bifacial modules with site mean albedo at Desert Rock, and 185 min for the bifacial modules with enhanced albedo at Boulder. The maximum duration based on I_{mp} is around half that based on I_{sc}. As we previously saw in Fig. 3, the 125% rule determines a low requirement when comparing to the 3 h maximum average for bifacial modules with enhanced albedo, so the long duration of the events is also related to having too low of a threshold, in proportional terms.

Lastly, the number of events per year gives an idea of maintenance frequency such as replacing diodes. For both I_{sc} and I_{mp}, Boulder leads for mono and bifacial modules, at either 25º or its optimal tilt setup. The maximum number of events for $I_{sc} > I_{125\%}$ are 291 for monofacial modules, 503 for bifacial with mean site albedo, and 1,816 for bifacial with enhanced albedo. Meanwhile, the maximum number of events for $I_{mp} > I_{125\%}$ are 71 for monofacial modules, 163 for bifacial with mean site albedo, and 1,224 for bifacial with enhanced albedo. The number of extreme events based on I_{mp} range between 24-67% of those based on I_{sc}.

Both the mean time over the 125% rule, the maximum duration of the extreme events, and the mean number of events per year help us to quantify the impact of the times where PV strings deliver a strong current, complementing the previously provided maximum short-circuit current and maximum power-point current. This is especially important for some sites. While Sioux Falls presented the strongest 1 min maximum values, now we see that those events are not as frequent as in other locations like Boulder. Additional parameters related to frequency could also be helpful for inverter selection if the goal was to minimize the total time of failure instead of no failure at all, or for choosing a tilt angle instead of a tracking system when working with bifacial modules.

IV. CONCLUSIONS

We analyzed the impact of overirradiance events on the current input for an inverter considering several configurations and sites in the US. The study also covered the effect of time resolution and averaging on the modeled results. We used 10 years of 1 minute solar data for 7 sites in the SURFRAD network, and modeled the short-circuit current using pvlib. Modeled currents were

compared with the industry standards NEC 2009 and NEC 2017, corresponding to the 125% rule and the 3 hour average maximum, respectively.

The maximum short-circuit current decreases with time resolution and averaging and the shape of the decay varies by site. The 3 hour average maximum short-circuit current is insensitive to the original data time resolution. The 1 minute maximum short-circuit current was the strongest at Sioux Falls for the 25º tilt and bifacial module with enhanced albedo, and it greatly surpassed the 125% rule for all cases. In some cases, the 1 minute maximum even surpassed the inverter nameplate maximum and panel fuses. For the bifacial modules with enhanced albedo, the 3 hour maximum was already greater than the 125% rule. This suggests that – even for coarse resolutions – 125% is not a suitable rule for selecting an inverter for bifacial modules. The frequency of the events over the 125% rule was largest at the sites with more solar resource: Boulder and Desert Rock. The longest extreme events were over 6 hour long for bifacial modules with enhanced albedo and tracking.

The current industry standards for selecting inverters based on the 125% rule or 3 hour averages do not prevent short and strong events of overirradiance from affecting the plant operation. While for monofacial modules the 3 hour average maximum less estrict than the 125% rule, this was not true for bifacial modules. If the goal was to create a rule that could prevent strong 1 minute events, either a 200% rule based on the module's short-circuit current or 1.5 times the 3 hour maximum average, which could be derived from hourly data, would prevent any large current events. Still, if 1 min resolution data is available, either from measurements or more recent satellite-derived commercial products, it will still be beneficial to do a high resolution simulation for a more informed design.

We would like to note that the analysis performed used data that represents the behavior of a single point in space. While a large solar plant is known to smooth the incoming strong irradiance by geographic diversity effect related to covering a large area, a single string might not represent significant geographic diversity to smooth the timeseries, and follow the results presented herein.

Lastly, recent works have covered the effect of inverter power-limiting control by deviating from the maximum-power point to higher voltage operating points[7,9]. While this might be a good operational solution for avoiding high currents in the future, it may also reduce the energy output, and existing PV plants with maximum-power tracking algorithms are likely to continue failing. Future work could add realism to these type of diagnostics by estimating the derating of fuses due to high temperatures.

ACKNOWLEDGMENTS

MZZ thanks the Faculty of Physical and Mathematical Sciences at Universidad de Chile for a faculty incorporation grant.

DATA AVAILABILITY STATEMENT

Solar data are available at the SURFRAD website: `https://gml.noaa.gov/aftp/data/radiation/surfrad/`. The code used in this study is available at `https://github.com/mzamora/InverterEnhancement`.

REFERENCES

[1]International Energy Agency, "Renewables 2021," Tech. Rep. (2021).

[2]L. R. do Nascimento, T. de Souza Viana, R. A. Campos, and R. Rüther, "Extreme solar overirradiance events: Occurrence and impacts on utility-scale photovoltaic power plants in Brazil," Solar Energy **186**, 370–381 (2019).

[3]Z. K. Pecenak, F. A. Mejia, B. Kurtz, A. Evan, and J. Kleissl, "Simulating irradiance enhancement dependence on cloud optical depth and solar zenith angle," Solar Energy **136**, 675–681 (2016).

[4]G. H. Yordanov, "A study of extreme overirradiance events for solar energy applications using NASA's I3RC Monte Carlo radiative transfer model," Solar Energy **122**, 954–965 (2015).

[5]C. A. Gueymard, "Cloud and albedo enhancement impacts on solar irradiance using high-frequency measurements from thermopile and photodiode radiometers. Part 1: Impacts on global horizontal irradiance," Solar Energy **153**, 755–765 (2017).

[6]G. H. Yordanov, O.-M. Midtgård, T. O. Saetre, H. K. Nielsen, and L. E. Norum, "Overirradiance (cloud enhancement) events at high latitudes," in *2012 IEEE 38th Photovoltaic Specialists Conference (PVSC) Part 2* (2012) pp. 1–7.

[7]M. Järvelä and S. Valkealahti, "Operation of a PV power plant during overpower events caused by the cloud enhancement phenomenon," Energies **13** (2020), 10.3390/en13092185.

[8]K. Lappalainen and S. Valkealahti, "Experimental observations about the cloud enhancement phenomenon on PV strings," in *8th World Conference on Photovoltaic Energy Conversion* (2022) pp. 1354 – 1358.

[9]K. Lappalainen and J. Kleissl, "Analysis of the cloud enhancement phenomenon and its effects on photovoltaic generators based on cloud speed sensor measurements," Journal of Renewable and Sustainable Energy **12**, 043502 (2020).

[10]L. Toreti Scarabelot, G. Arns Rampinelli, and C. R. Rambo, "Overirradiance effect on the electrical performance of photovoltaic systems of different inverter sizing factors," Solar Energy **225**, 561–568 (2021).

[11]J. Luoma, J. Kleissl, and K. Murray, "Optimal inverter sizing considering cloud enhancement," Solar energy **86**, 421–429 (2012).

[12]M. Zamora Zapata, E. Wu, and J. Kleissl, "Irradiance enhancement events in the coastal stratocumulus dissipation process," in *Solar World Congress, Santiago, Chile, International Solar Energy Society* (2019).

[13]R. Kharait, S. Raju, A. Parikh, M. A. Mikofski, and J. Newmiller, "Energy yield and clipping loss corrections for hourly inputs in climates with solar variability," in *2020 47th IEEE Photovoltaic Specialists Conference (PVSC)* (2020) pp. 1330–1334.

[14]A. Parikh, K. Perry, K. Anderson, W. B. Hobbs, R. Kharait, and M. A. Mikofski, "Validation of subhourly clipping loss error corrections," in *2021 IEEE 48th Photovoltaic Specialists Conference (PVSC)* (2021) pp. 1670–1675.

[15]K. Anderson and K. Perry, "Estimating subhourly inverter clipping loss from satellite-derived irradiance data," in *2020 47th IEEE Photovoltaic Specialists Conference (PVSC)* (2020) pp. 1433–1438.

[16]C. Ladd, "Simulating NEC voltage and current values," Solar professional magazine , 12–18 (2008).

[17]J. Stein, C. Reise, J. B. Castro, G. Friesen, G. Maugeri, E. Urrejola, and S. Ranta, "Bifacial photovoltaic modules and systems: Experience and results from international research and pilot applications," Tech. Rep. (IEA, 2021).

[18]S. Ayala Pelaez, C. Deline, P. Greenberg, J. S. Stein, and R. K. Kostuk, "Model and validation of single-axis tracking with bifacial PV," IEEE Journal of Photovoltaics **9**, 715–721 (2019).

[19]LG, "Bifacial design guide," Tech. Rep. (2017).

[20]B. Marion, "Albedo data sets for bifacial PV systems," in *2020 47th IEEE Photovoltaic Specialists Conference (PVSC)* (2020) pp. 0485–0489.

[21]Solar World, "Calculating the additional energy yield of bifacial solar modules," (2016).

[22]W. F. Holmgren, C. W. Hansen, and M. A. Mikofski, "pvlib python: a python package for modeling solar energy systems," Journal of Open Source Software **3**, 884 (2018).

[23]M. A. Anoma, D. Jacob, B. C. Bourne, J. A. Scholl, D. M. Riley, and C. W. Hansen, "View factor model and validation for bifacial PV and diffuse shade on single-axis trackers," in *2017 IEEE 44th Photovoltaic Specialist Conference (PVSC)* (2017) pp. 1549–1554.

[24]A. Castillejo-Cuberos and R. Escobar, "Understanding solar resource variability: An in-depth analysis, using Chile as a case of study," Renewable and Sustainable Energy Reviews **120**, 109664 (2020).

[25]M. Zamora Zapata and J. Kleissl, "Dependence of subhourly solar variability statistics on time interval and cloud vertical position," Journal of Renewable and Sustainable Energy **14**, 036501 (2022).

Appendix A: Complementary statistics for I_{mp}

The following Figs. 6 and 7 represent the same behavior shown for I_{sc} in Figs. 2 and 3 but for the modeled maximum-power point current I_{mp}.

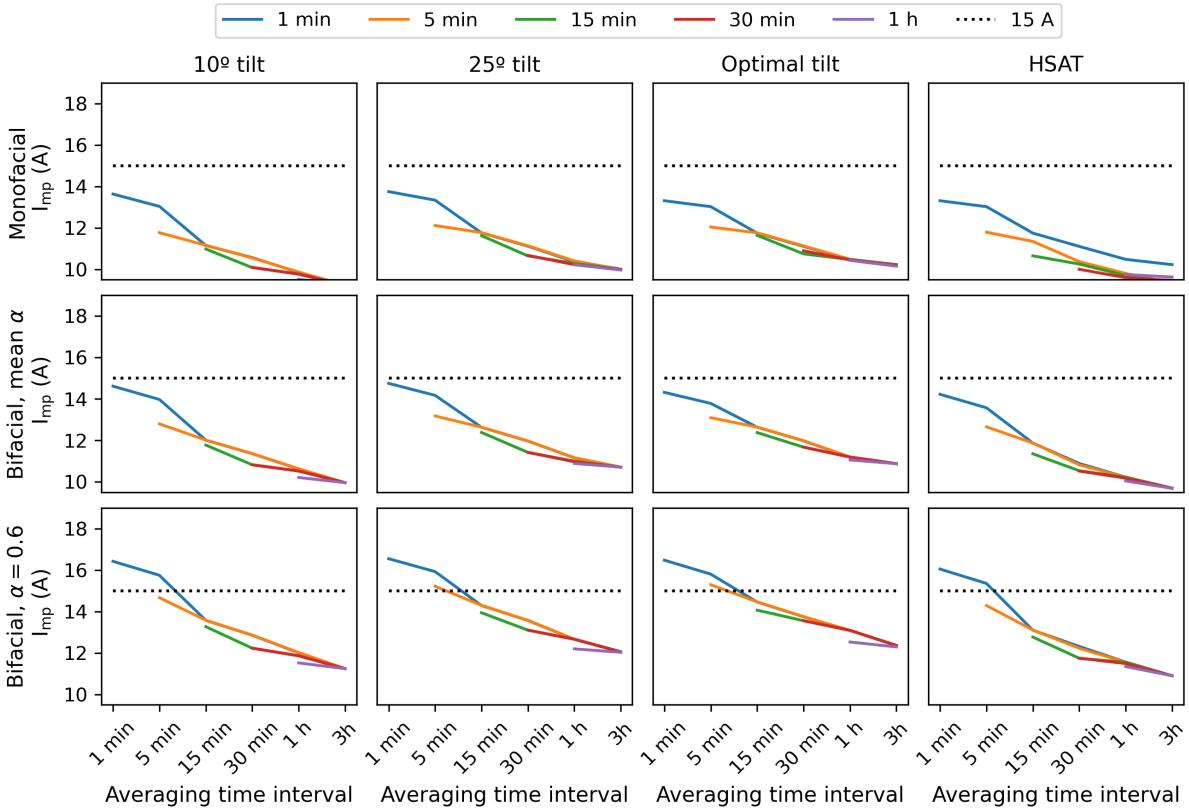

FIG. 6. Maximum current at the maximum-power point I_{mp} for Sioux Falls, obtained from the different downsampled timeseries (1 min to 1 h), are shown as a function of the averaging time window (1 min to 3 h).

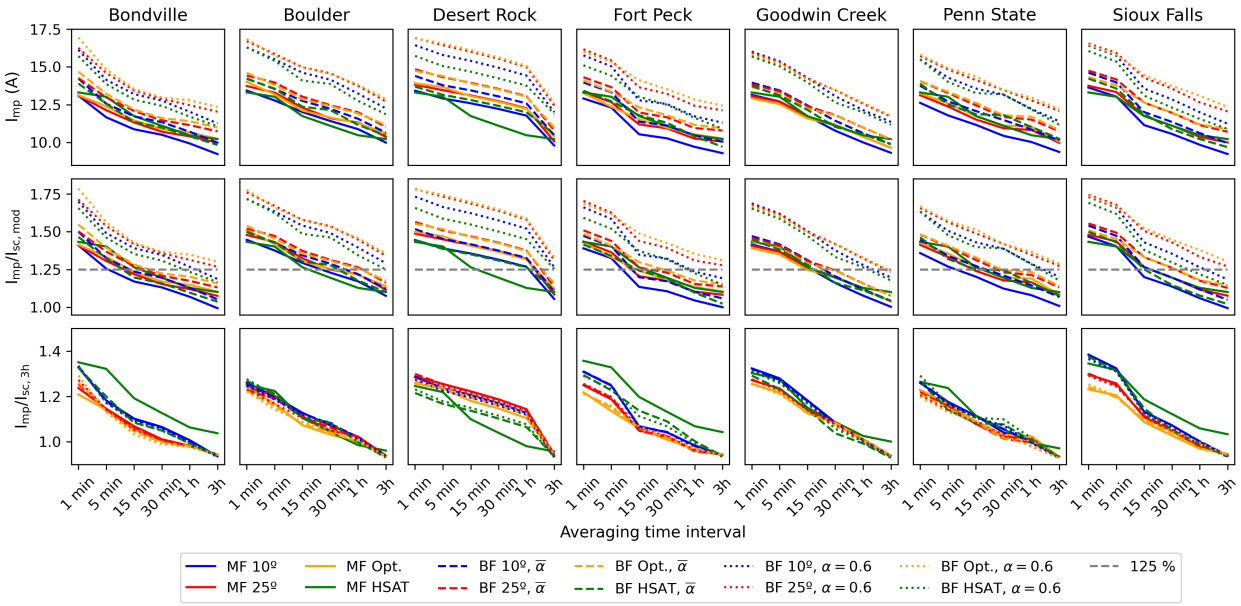

FIG. 7. Maximum current at the maximum-power point I_{mp} as a function of the averaging time window per site, using the 1 minute resolution data. The top row shows the absolute values highlighting the 15 A in dashed gray, the middle row shows the values normalized by the module short-circuit current $I_{sc,mod}$, and the bottom row shows the values normalized by $I_{sc,3h}$.